AMERICAN SOCIETY FOR MICROBIOLOGY | mBio®

RESEARCH ARTICLE

Host-Primed Ebola Virus GP Exposes a Hydrophobic NPC1 Receptor-Binding Pocket, Revealing a Target for Broadly Neutralizing Antibodies

Zachary A. Bornholdt,[a] Esther Ndungo,[b] Marnie L. Fusco,[a] Shridhar Bale,[a] Andrew I. Flyak,[c] James E. Crowe, Jr.,[c,d,e] Kartik Chandran,[b] Erica Ollmann Saphire[a,f]

Department of Immunology and Microbial Science, The Scripps Research Institute, La Jolla, California, USA[a]; Department of Microbiology and Immunology, Albert Einstein College of Medicine, Bronx, New York, USA[b]; Department of Pathology, Microbiology and Immunology,[c] Department of Pediatrics,[d] and Vanderbilt Vaccine Center,[e] Vanderbilt University, Nashville, Tennessee, USA; The Skaggs Institute for Chemical Biology, The Scripps Research Institute, La Jolla, California, USA[f]

Z.A.B. and E.N. contributed equally to this article.

This is manuscript number 29196 from The Scripps Research Institute.

ABSTRACT **The filovirus surface glycoprotein (GP) mediates viral entry into host cells. Following viral internalization into endosomes, GP is cleaved by host cysteine proteases to expose a receptor-binding site (RBS) that is otherwise hidden from immune surveillance. Here, we present the crystal structure of proteolytically cleaved Ebola virus GP to a resolution of 3.3 Å. We use this structure in conjunction with functional analysis of a large panel of pseudotyped viruses bearing mutant GP proteins to map the Ebola virus GP endosomal RBS at molecular resolution. Our studies indicate that binding of GP to its endosomal receptor Niemann-Pick C1 occurs in two distinct stages: the initial electrostatic interactions are followed by specific interactions with a hydrophobic trough that is exposed on the endosomally cleaved GP_1 subunit. Finally, we demonstrate that monoclonal antibodies targeting the filovirus RBS neutralize all known filovirus GPs, making this conserved pocket a promising target for the development of panfilovirus therapeutics.**

IMPORTANCE **Ebola virus uses its glycoprotein (GP) to enter new host cells. During entry, GP must be cleaved by human enzymes in order for receptor binding to occur. Here, we provide the crystal structure of the cleaved form of Ebola virus GP. We demonstrate that cleavage exposes a site at the top of GP and that this site binds the critical domain C of the receptor, termed Niemann-Pick C1 (NPC1). We perform mutagenesis to find parts of the site essential for binding NPC1 and map distinct roles for an upper, charged crest and lower, hydrophobic trough in cleaved GP. We find that this 3-dimensional site is conserved across the filovirus family and that antibody directed against this site is able to bind cleaved GP from every filovirus tested and neutralize viruses bearing those GPs.**

Received 31 December 2015 **Accepted** 8 January 2016 **Published** 23 February 2016

Citation Bornholdt ZA, Ndungo E, Fusco ML, Bale S, Flyak AI, Crowe JE, Jr, Chandran K, Saphire EO. 2016. Host-primed Ebola virus GP exposes a hydrophobic NPC1 receptor-binding pocket, revealing a target for broadly neutralizing antibodies. mBio 7(1):e02154-15. doi:10.1128/mBio.02154-15.

Editor Peter Palese, Icahn School of Medicine at Mount Sinai

Address correspondence to Kartik Chandran, kartik.chandran@einstein.yu.edu, and Erica Ollmann Saphire, erica@scripps.edu.

This article is a direct contribution from a Fellow of the American Academy of Microbiology. External solicited reviewers: Thomas Geisbert, University of Texas Medical Branch; Benhur Lee, Icahn School of Medicine at Mount Sinai.

Ebola virus (EBOV) and Marburg virus (MARV) are both members of the *Filoviridae* family of enveloped negative-strand RNA viruses and are the causative agents of a highly lethal disease for which no approved vaccines or treatments are currently available (1, 2). Due to their virulence and biothreat potential, filoviruses are classified as category A pathogens. The ongoing EBOV epidemic in West Africa is the longest and most widespread filovirus outbreak on record (3).

Like all filoviruses, EBOV displays a single virus-encoded protein, the viral glycoprotein (GP), on the surface of the virion. EBOV GP is a 676-residue class I membrane fusion glycoprotein. However, EBOV GP differs from canonical class I fusion proteins, such as those of human immunodeficiency virus and influenza A virus, in that the architecture of its fusion loop more closely resembles those of class II and III glycoproteins (4, 5). EBOV GP is synthesized as a precursor polypeptide, GP_0, which assembles into trimers in the endoplasmic reticulum. Each GP_0 subunit is then posttranslationally cleaved by the Golgi endoprotease furin to yield disulfide-linked GP_1 (≈55 kDa) and GP_2 (≈20 kDa) subunits. The final GP assembly, which is an ≈450 kDa trimer of $GP_{1,2}$ heterodimers, is then displayed on the surface of mature EBOV virions (4, 5). GP_1 contains the receptor-binding site and regulates the triggering of the membrane fusion machinery in the GP_2 subunit (6).

The GP_1 structure can be divided into three subdomains: the mucin domain, glycan cap, and GP_1 core. The outer mucin domain (GP_1 residues 313 to 464), is predicted to be loosely structured and heavily glycosylated, incorporating five N-linked gly-

cans and 12 to 17 predicted O-linked glycans (5). Interior to the mucin-like domain is the glycan cap (GP_1 residues 227 to 313), which sits atop the GP_1 core. The glycan cap is more ordered than the mucin-like domain and contains four N-linked glycosylation sites. Neither the mucin nor the glycan cap domain is essential for viral entry. Indeed, removal of these domains enhances infection by viruses pseudotyped with EBOV GP (7–9). Therefore, it is currently hypothesized that a primary function of the mucin domain and glycan cap is to shield the GP_1 core from immune surveillance (4, 5, 10, 11).

EBOV virions are internalized into cells via a macropinocytosis-like mechanism and undergo trafficking to late endosomes (12–15). There, host endosomal cysteine proteases, including cathepsins L (CatL) and B (CatB), cleave GP_1 to remove the mucin and glycan cap domains. Cleavage generates a fusion-competent GP trimer (GP_{CL}) comprising the 19-kDa GP_1 core domain and GP_2 (8, 9, 16). Cleavage of $GP_{1,2}$ to GP_{CL} is a prerequisite for viral recognition of the host endosomal receptor Niemann-Pick C1 (NPC1) (10, 17–20), strongly suggesting that the receptor-binding site in the GP_1 core structure is unmasked by the cleavage of GP_1 in late endosomes. Thus, GP_{CL} represents the structure of EBOV GP in a conformation that is competent for receptor binding.

In order to observe possible structural changes in GP_{CL} and to illustrate definitively which surfaces and residues are unveiled upon endosomal proteolysis, we determined the crystal structure of the EBOV GP_{CL} trimer at a resolution of 3.3 Å, in complex with the neutralizing human antibody Fab KZ52 (21). We found that the main feature exposed upon priming of EBOV GP is a wave-like morphology at the top of GP_{CL}, with a polar/basic crest rising above a large, recessed, hydrophobic trough, previously occupied by the glycan cap prior to priming by host cathepsins. Extensive structure-directed mutagenesis of EBOV GP_{CL} revealed that the basic character of the polar crest is crucial to the EBOV-receptor interaction, likely because it confers an initial electrostatic attraction between GP_{CL} and the second luminal domain of NPC1, domain C. We also find that the trough makes specific hydrophobic contacts that are essential to high-affinity GP_{CL}-NPC1 domain C binding. Finally, we demonstrate that host-programmed unmasking of the NPC1-binding site in EBOV GP creates a broadly conserved target for neutralization by monoclonal antibodies (MAbs) recently isolated from a human survivor of MARV infection (22). Our results thus suggest a novel approach for developing engineered MAbs with broad-spectrum activity against filoviruses.

RESULTS

The crystal structure of EBOV GP_{CL} reveals the NPC1 receptor-binding site that is unmasked upon endosomal cleavage. Purified EBOV $GP_{1,2}$ ectodomains (expressed without mucin-like domains; hereinafter referred to as GP) were treated with thermolysin, which mimics host endosomal protease processing of EBOV GP (8), in order to generate EBOV GP_{CL} trimers for crystallization. EBOV GP_{CL} crystallizes in the space group H3 (R3:H) with four GP monomers and four KZ52 Fabs in the asymmetric unit (ASU). The ASU contains one full GP trimer and one remaining GP monomer, which itself forms a biologically relevant trimer with two symmetry-related protomers about a crystallographic 3-fold axis. The overall changes to the tertiary structure upon cleavage of GP are minimal, reflected in a root mean square deviation (RMSD) of 0.419 Å compared to the structure of uncleaved EBOV GP (Fig. 1A) (4). This finding corroborates a previous model of EBOV GP_{CL} which suggested only limited changes in the GP_{CL} structure upon thermolysin digestion (23). The structure of EBOV GP_{CL} is more compact than that of EBOV GP and exhibits more stable crystal packing, less disorder, and improved resolution of X-ray diffraction over that of the previously determined uncleaved GP (4).

New regions of EBOV GP can now be visualized in the EBOV GP_{CL} structure. These include C-terminal residues of GP_2, the disulfide link between C53 of GP_1 and C609 of GP_2, and an intra-GP_2 disulfide bond between C601 and C610. As EBOV GP_2 descends from the base of the GP trimer structure, it forms a tightly ordered loop structure that is stabilized by the intra-GP_2 disulfide bond between C601 and C610. This disulfide link turns the peptide chain back toward the body of GP where it is anchored to GP_1 by the C53-C609 inter-$GP_{1,2}$ disulfide bond prior to turning downward toward the transmembrane domain and viral membrane (Fig. 1B).

The most striking structural feature of GP_{CL} is the full exposure of a charged hydrophilic crest and a large hydrophobic trough structure in immediate proximity to the GP_2 fusion loop. The trough becomes exposed upon proteolytic excision of the glycan cap from EBOV GP and is 13 Å wide, 23 Å long, and 10 Å deep (Fig. 1C). Residues I113 and L111 form an exposed hydrophobic face inside the trough, while residues V79, T83, W86, F88, L122, V141, and I170 line the bottom of the trough.

Mutation of GP residues exposed after removal of the glycan cap affects viral infectivity and binding to the filovirus receptor NPC1. Previous work utilizing scanning mutagenesis of EBOV GP identified multiple residues important for viral infectivity (24–26). These studies were carried out prior to the availability of a crystal structure of EBOV GP (4) or GP_{CL} (this work) and prior to identification of the endosomal receptor, NPC1 (17, 18). Here, we map these residues onto the crystal structure of EBOV GP_{CL} and determine whether mutations in EBOV GP that reduce infectivity specifically correlate with defects in GP_{CL}-NPC1 binding. Previous work identified three lysines at positions 114, 115, and 140 (16, 25) and hydrophobic residues F88, L111, and L122 (25–27) for which mutation to alanine diminishes infectivity (16, 25). These deficits in infectivity correlate with reductions in NPC1 binding, as determined by co-immunoprecipitation (28).

The crystal structure of EBOV GP_{CL} illustrates that K114, K115, and K140 lie along the crest and F88, L111, and L122 line the trough of EBOV GP_{CL}. These hydrophobic residues are buried in uncleaved EBOV GP (4) but become solvent exposed in the trough of EBOV GP_{CL}. We systematically mutated residues that the GP_{CL} crystal structure shows to be surface-exposed after cleavage, in order to determine their importance for NPC1 binding and viral infectivity and to define the GP_1 receptor-binding site (RBS).

We pseudotyped vesicular stomatitis virus (VSV) particles with 73 mutant GP proteins and tested them for viral incorporation of GP relative to the incorporation of the wild-type (WT) protein, and for binding to the conformational antibody KZ52 (4, 21), which only recognizes properly folded GP (see Fig. S4 in the supplemental material). The 68 VSV-GP mutants that met these quality benchmarks were then evaluated for their capacity to recognize a purified, soluble form of human NPC1 domain C in an

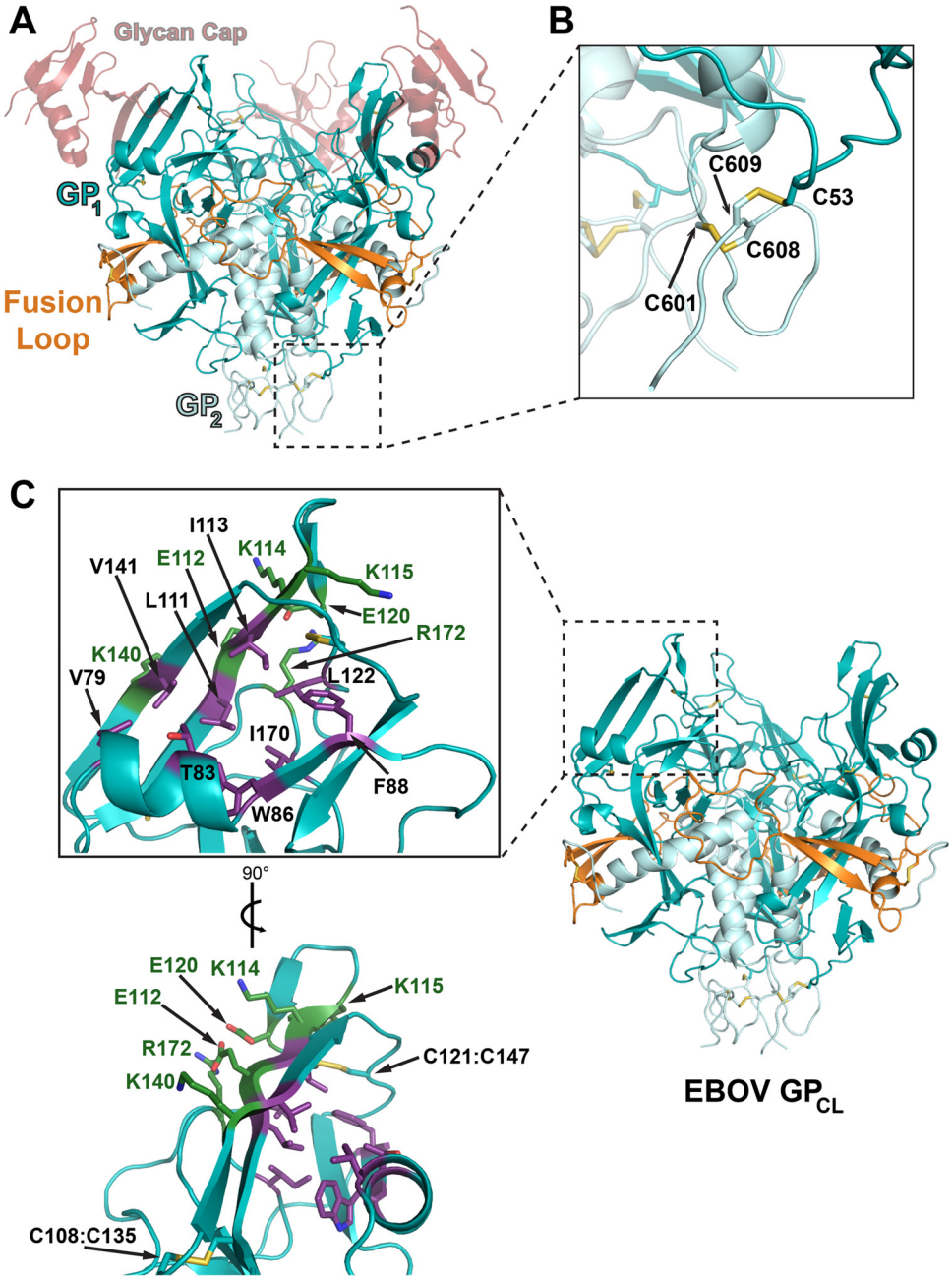

FIGURE 1 Crystal structure of ebolavirus GP_{CL}. (A) The trimeric EBOV GP_{CL} structure is shown, with GP_1 colored teal, GP_2 colored light blue, the fusion loop colored orange, and disulfide bonds displayed as sticks and colored gold. The former position of the glycan cap, now absent in the GP_{CL} structure, is illustrated in semitransparent red and is derived from an alignment with the uncleaved EBOV GP structure (PDB code 3CSY). (B) Additional residues at the C terminus of GP_2 are now visible in this higher-resolution structure. These residues include C601-C608, contained within GP_2, as well as the C53-C609 disulfide bond that cross-links GP_1 and GP_2 together. (C) The structure of EBOV GP_{CL} is displayed to the right, with the same coloring as described for panel A. An enlarged illustration of the putative EBOV GP_1 RBS is shown to the left, in two orientations. Residues forming the hydrophilic crest and hydrophobic trough are labeled and colored green and purple, respectively. The disulfide bonds present around the crest and trough, C108-C135 and C121-C145, are colored gold.

enzyme-linked immunosorbent assay (ELISA), as described previously (27, 29). We report that WT EBOV GP_{CL} binds to NPC1 domain C with a 50% effective concentration (EC_{50}) of ≈0.5 nM, consistent with a high-avidity binding interaction between these proteins. In comparison, we find that mutants that demonstrate reduced infectivity are also defective for binding to NPC1 domain C (see Fig. S1 and S2 in the supplemental material). Furthermore, a few single point mutations that cause drastic reductions (>10-fold) in the GP_{CL}-NPC1 domain C-binding EC_{50} are located in or around the hydrophobic trough and hydrophilic crest. These mutants allow us to map those residues of EBOV GP_1 that are critical to NPC1 domain C onto the EBOV GP_{CL} structure and to better

define the RBS (see Fig. S1 and S2). Interestingly, mutation to alanine of two trough residues, F88 and L111, reduces viral infectivity dramatically (by >3 $\log_{10}$ units) but has more modest effects on GP_{CL}-NPC1 binding (see Fig. S2A). The disparity between strong reduction in infectivity but modest effect on NPC1 binding suggests that these residues may be important for steps in viral entry post-NPC1 binding and prior to membrane fusion, such as conformational changes or release of GP2.

The hydrophobic trough exposed on GP1 upon endosomal cleavage is the primary binding site of NPC1 domain C. We performed further mutagenesis of the hydrophobic trough to better define its precise role. Since most of the point mutations to alanine within the hydrophobic trough had only modest effects, we postulated that replacing them with bulkier methionine residues would more completely occlude the trough and prevent GP-NPC1 binding. We selected two trough residues, T83 and I113, which did not inhibit NPC1 binding when mutated to alanine, for additional mutagenesis to methionine (Fig. 2A and B). To prevent misfolding or disruption of the GP structure, we engineered compensatory mutations with interacting residues of the glycan cap to fit the larger methionine residues and prevent steric clashing. We engineered the following mutants: I113M (trough)/F225A (cap), T83M (trough)/F225V+Y232F (cap), and T83M+I113M (trough)/F225A+Y232F (cap) (Fig. 2C to E). For simplicity, since the compensatory mutations are removed along with the glycan cap upon proteolysis, we will only refer to these mutants by the mutations remaining on EBOV GP_{CL}: T83M, I113M, and T83M+I113M. All engineered VSV-GP mutants maintain high levels of incorporation compared to the incorporation of WT GP (see Fig. S2 in the supplemental material). As posited, the single T83M and I113M mutations, as well as the T83M+I113M double mutation, lead to defects in NPC1 domain C binding and pseudovirus infectivity by GP_{CL} bearing them (Fig. 2A to C). We further find that a single point mutation, L122A, located in the bottom of the trough, abrogates both NPC1 domain C binding and pseudotyped virus infectivity (Fig. 2E). The position of L122 suggests that it has a structural role; the L122A mutation may destabilize the local trough structure, preventing NPC1 binding and subsequent infectivity. Together, these findings provide evidence that supports a direct correlation between NPC1 binding and infectivity and effectively maps the GP_{CL} trough as a critical component of the NPC1-binding site.

An overall basic charge on the GP_1 crest is required for GP binding to NPC1 domain C and viral infectivity. Experiments performed prior to the identification of the filovirus endosomal receptor NPC1 demonstrated that K114A, K115A, and K140A mutations (now mapped to the GP_{CL} crest) significantly reduce viral infectivity (16, 25). Here, we investigated whether the observed reductions in viral infectivity from these mutations correlate with defects in binding to NPC1 domain C. We show that while the individual mutations K114A and K115A have only modest effects (see Fig. S1 and S2 in the supplemental material), the double mutation (K114A+K115A) dramatically inhibits GP_{CL}-NPC1 domain C binding and viral entry (Fig. 3A and B). In contrast, the K140A mutant showed no significant defect in viral infectivity or NPC1 domain C binding (see Fig. S2). To test the hypothesis that these crest residues participate in electrostatic interactions with NPC1 during virus-receptor engagement, we engineered and analyzed VSV-GPs in which these lysines were replaced with either basic or acidic residues. The K114R+K115R double mutant, which maintains the basic charge, remains fully functional. In contrast, the K114E+K115E double mutant, which reverses charge, displays an even greater deficit in receptor-binding function and entry activity than the neutral K114A+K115A mutant (Fig. 3A and B). To determine whether it is the overall charge of the site or specific basic residues within the site that are important, we mutated two glutamic acid residues in proximity to positions 114 and 115 to alanine. The resulting quadruple mutant (K114A+K115A+E112A+E120A), which is predicted to have WT-like electrostatics, exhibits receptor-binding activity and infectivity at nearly WT levels (Fig. 3A and B). The importance of a set of basic residues but lack of a specific requirement for any one of them individually suggest a need to maintain an overall basic charge on the GP_{CL} crest (Fig. 3C).

Neutralizing antibodies raised from a Marburg virus survivor demonstrate potential panfilovirus neutralization activity. The high degree of sequence and structural conservation in the NPC1-binding site of filovirus glycoproteins makes it an attractive target for the development of broadly neutralizing MAbs with therapeutic potential (see Fig. S3 in the supplemental material). Unfortunately, no such MAbs against ebolaviruses have been isolated. Instead, most known neutralizing anti-ebolavirus MAbs target a conformational epitope at the base of the $GP_{1,2}$ trimer (4, 5, 30, 31). Recently, however, several MAbs isolated from a human survivor of MARV infection were found to recognize the hydrophobic GP_{CL} trough and inhibit GP-NPC1 domain C binding (11, 22). Of significance, one anti-MARV MAb from that study, MR72, cross-reacts with purified GP and GP_{CL} of EBOV, while three other MAbs, MR78, MR111, and MR191, cross-react only with EBOV GP_{CL} (22). MR72, MR78, MR111, and MR191 bind to similar locations on MARV GP but approach from significantly different angles (22). The third complementarity-determining region of the heavy chain variable region (CDRH3) of MR78 binds into the expected MARV GP_1 RBS (see Fig. S3) (11).

As the RBS is conserved in sequence and structure across known filoviruses, we evaluated the capacity of MR72 and two additional GP_{CL}-reactive antibodies, MR78 and MR191 (22), to recognize and neutralize VSV bearing GP_{CL} from four ebolaviruses (Sudan virus [SUDV], Bundibugyo virus [BDBV], Taï Forest virus [TAFV], and Reston virus [RESTV]) and the cuevavirus Lloviu virus (LLOV) (2, 32). Remarkably, we find that MR72 effectively neutralizes VSVs pseudotyped with GP_{CL} derived from all known filoviruses (Fig. 4A). In contrast, MR191 neutralizes VSV bearing other filovirus GPs only weakly, and MR78 fails to neutralize VSVs bearing GP_{CL} derived from any species other than MARV. We speculate that the steeper angle of approach of MR191 to MARV GP_{CL} compared to that of MR78 may enhance the breadth of neutralization by improving access to the shared RBS (Fig. 4A and S3). Of significance, we found that MR72 failed to bind VSVs bearing uncleaved EBOV GP on the surface (see Fig. S3 in the supplemental material). This finding is in contrast to a previous observation of MR72 binding to uncleaved soluble EBOV GP ectodomain (see Fig. S3) (22). It is likely that there are differences in the presentation of EBOV GP on the surface of actual virions that prevent MR72 from binding and effectively neutralizing either wild-type EBOV or VSV bearing uncleaved EBOV GP.

The contrasting neutralization breadth properties of MR72 and MR78, despite their similar binding angles and shared epitope, led us to explore our panel of GP_{CL} mutations to identify

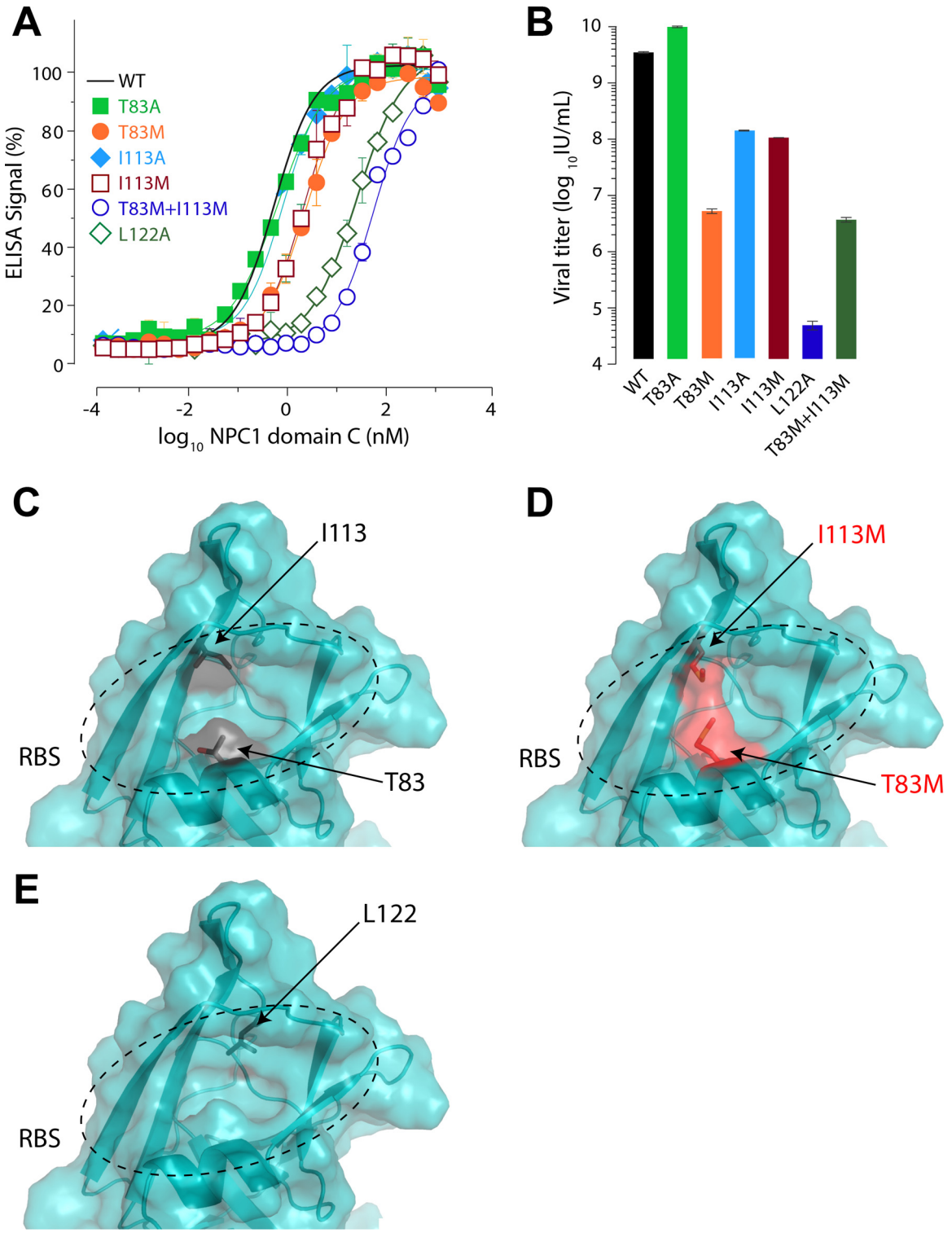

FIGURE 2 Mutagenic occlusion of the EBOV GP_1 receptor-binding site. (A) Alanine or methionine mutations were made to key residues in the RBS. The affinities of wild-type and mutant GP_{CL} for NPC1 domain C were analyzed via ELISA. Note that the L122A and T83M+I113M mutations significantly reduce binding to NPC1 domain C. Means ± SD ($n = 4$) from a representative experiment are shown. (B) Graph displaying titers of VSV pseudoviruses harboring GP_1 RBS mutations. Means ± SD ($n = 2–4$) from a representative experiment are shown. (C) A semitransparent surface has been placed over the cartoon model of the WT RBS on EBOV GP_1 to display the RBS pocket (within the dashed oval outline). Residues T83 and I113 are illustrated as sticks (black). (D) Model of EBOV RBS bearing the mutations T83M and I113M (red). The longer side chains of the introduced methionine residues fill the RBS pocket and likely prevent NPC1 domain C binding by occluding the NPC1 binding site. (E) The buried location of L122 (black) is displayed in the EBOV GP_1 RBS. See also Fig. S1, S2, and S4 in the supplemental material.

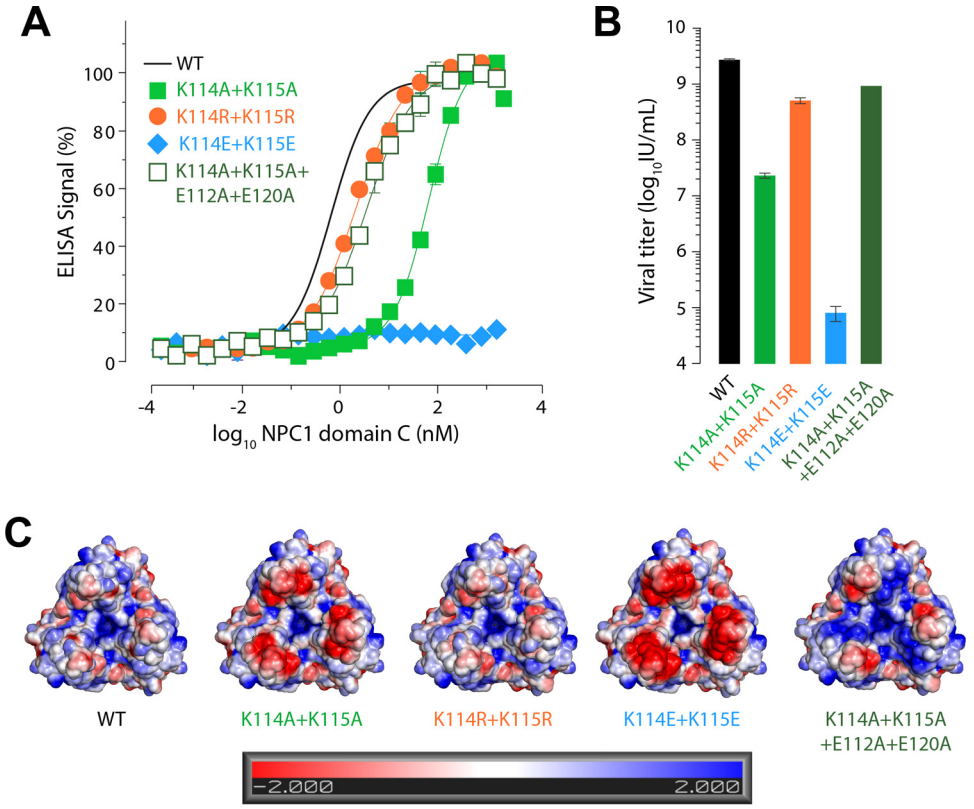

FIGURE 3 The basic electrostatic potential of the GP_1 crest is vital to receptor binding. (A) ELISA analysis of binding of wild-type or mutant GP_{CL} to NPC1 domain C. Replacement of positively charged K114 and K115 with neutral alanines or negatively charged glutamic acids reduces and abrogates NPC1 binding, respectively. Concomitant mutation of neighboring E112 and E120 to neutral alanine residues restores affinity for NPC1 domain C. Means ± SD ($n = 4$) from a representative experiment are shown. (B) Growth titers of VSV pseudotyped with electrostatic mutants of EBOV GP correlate with the NPC1 domain C affinities shown by the results in panel A: reduction in growth correlates with loss of positive charge. Means ± SD ($n = 2–4$) from a representative experiment are shown. (C) The electrostatic surface potential is calculated for each of the mutant EBOV GPs using APBS in PyMol (The PyMOL Molecular Graphics System, version 1.5.0.4. [Schrödinger, LLC], and APBS plugin for PyMol, M. G. Lerner and H. A. Carlson, University of Michigan, Ann Arbor, MI, 2006; 48). The view is looking down onto the EBOV GP trimer. Mutants with an overall negative charge on the surface of GP_1 demonstrate defects in both affinity for NPC1 domain C and viral growth. See also Fig. S1, S2, and S4 in the supplemental material.

specific residues in the GP RBS that can affect MR78's neutralization of EBOV GP_{CL} (see Fig. S2 in the supplemental material). We find that a single point mutation, V79A, allows MR78 to neutralize EBOV GP_{CL}: although MR78 cannot neutralize VSV bearing wild-type EBOV GP_{CL}, it can neutralize V79A-bearing VSV-EBOV GP_{CL} (Fig. 4B). Position 79 in EBOV GP is equivalent to position 63 in MARV. Structural alignment of EBOV GP_{CL} with MARV in the MARV GP-MR78 crystal structure (11) suggests that the wild-type V79 may sterically clash with the light chain of MR78. Replacement of valine with the smaller alanine residue (V79A) may improve neutralization by relieving the steric clash (Fig. 4B).

Furthermore, previous studies have shown that, unlike MR72, MR78 fails to block NPC1 domain C binding to EBOV GP_{CL} (11). Therefore, we performed NPC1 domain C competitive-binding assays to determine whether MR78 neutralizes EBOV GP_{CL}-V79A by inhibiting GP-NPC1 binding. Curiously, even though MR78 is now able to neutralize VSV bearing EBOV GP_{CL}-V79A, it remains unable to prevent binding of NPC1 domain C to EBOV GP_{CL} or EBOV GP_{CL}-V79A (Fig. 4B). MR72, however, does block NPC1 binding to EBOV GP_{CL}. Therefore, our data suggest that MAbs MR72 and MR78 may neutralize by distinct mechanisms. MR72 effectively blocks GP_{CL}-NPC1 binding for all filoviruses, whereas MR78 does not block EBOV GP_{CL}-NPC1 binding. We speculate that MR78 neutralizes EBOV entry by inhibiting viral membrane fusion downstream from virus receptor recognition.

In order to gauge the neutralization potentials of MR72 and MR78 relative to those of other MAbs with demonstrated protective efficacy *in vivo*, we performed a comparative analysis with the combined MAbs of the EBOV-specific ZMapp cocktail: 2G4, 4G7, and 13C6 (31, 33), as well as with KZ52, a known neutralizing MAb from a human survivor (21). Our analysis demonstrates that MR72 can neutralize pseudoviruses at 10-fold lower concentrations of antibody than are required for KZ52 and the ZMapp cocktail (Fig. 4C). Thus, MAbs such as MR72, which target the highly conserved GP_1 RBS, represent a novel avenue for both broad and potent neutralization of filoviruses, if they can be delivered to the endosomal compartments where GP_{CL} is generated during entry.

DISCUSSION

In this study, we present the 3.3-Å crystal structure of thermolysin-cleaved EBOV GP (GP_{CL}), which is primed for interaction with the filovirus receptor, NPC1. Thermolysin has previously been demonstrated to mimic host CatB and CatL proteolytic processing of

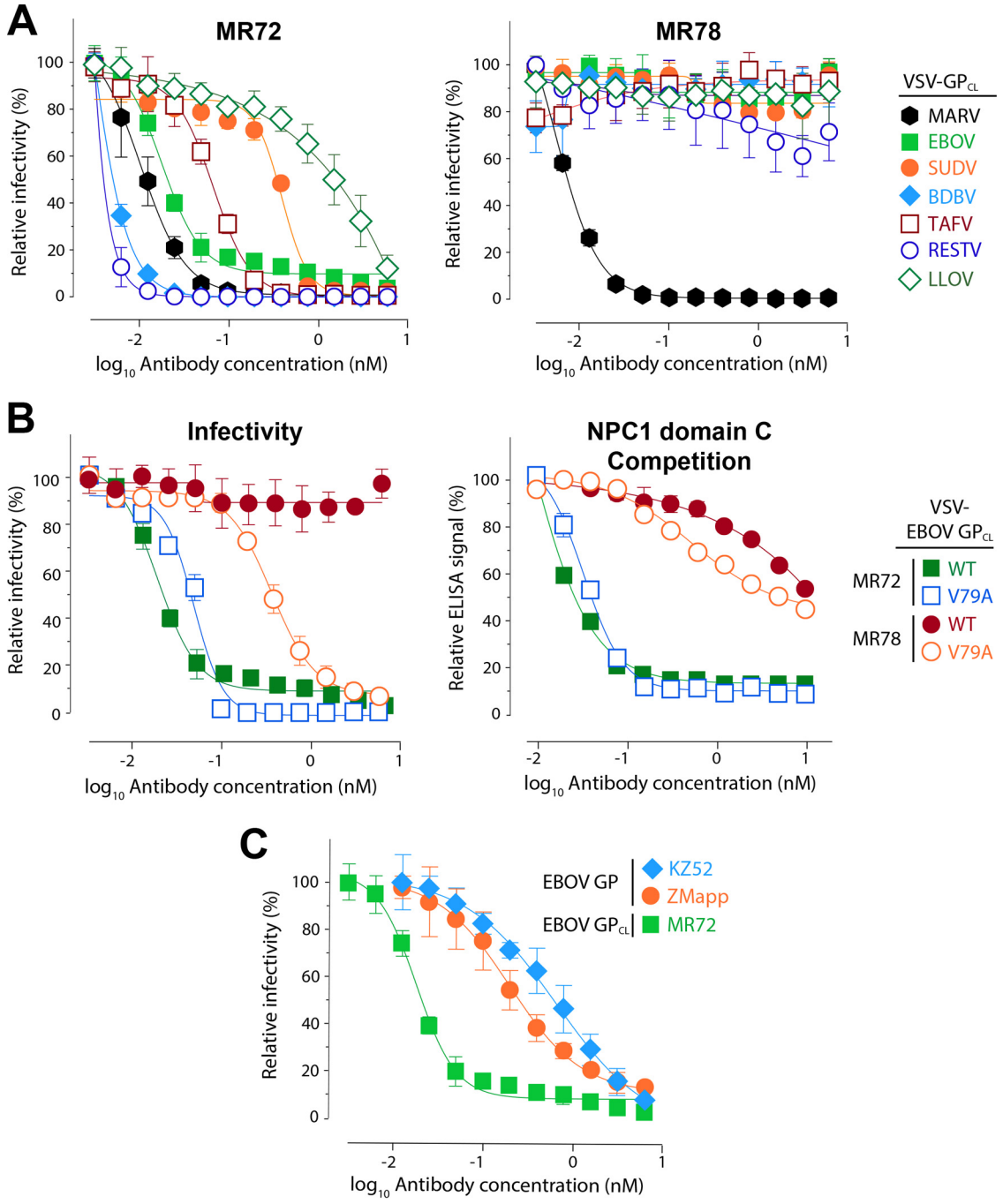

FIGURE 4 Monoclonal antibodies targeting the conserved GP_1 RBS demonstrate panfilovirus neutralization activity. (A) VSV pseudotyped with GPs from different species of filovirus (as indicated in the key to the right) were preprimed with thermolysin to expose the GP_1 RBS and then analyzed for reduction in relative infectivity following treatment with MR72 or MR78. (B) The graph to the left shows a comparative analysis of the neutralization of VSV-EBOV GP_{CL} and VSV-EBOV GP_{CL}-V79A by MR72 and MR78. The graph to the right displays the results of competitive binding assays detecting NPC1 domain C binding in the presence of increasing concentrations of MR72 or MR78 for EBOV GP_{CL} and EBOV GP_{CL}-V79A. The key for both graphs is on the far right. (C) Graph showing the results of comparative infectivity assays of nonprimed VSV pseudotyped with EBOV GP treated with MAbs from the ZMapp cocktail (2G4, 4G7, and 13C6) (33) or the neutralizing EBOV antibody KZ52 (21). MR72 neutralizes primed EBOV GP_{CL} pseudovirions at >10-fold lower concentrations than are required for ZMapp or KZ52 to neutralize EBOV GP pseudovirions. See also Fig. S3 in the supplemental material. Means ± SD ($n = 2-4$) from a representative experiment are shown in each panel.

EBOV GP, which occurs in the endosome and is required for receptor binding and membrane fusion (8–10, 16). This high-resolution structure of EBOV GP_{CL} has now defined the intermolecular disulfide bridge between C53 in GP_1 and C609 in GP_2, a region previously unresolved for EBOV GP. The disulfide bridge likely contributes to the inherent stability of ebolavirus GP despite proteolytic processing. This stability is reflected in a high degree of structural conservation between uncleaved EBOV GP (4) and

GP_{CL}; the aligned structures have an RMSD of 0.419 Å. The crystal structure of EBOV GP_{CL} presented here also illustrates how proteolytic priming removes the glycan cap of EBOV GP_1 to expose the binding site for the filovirus receptor NPC1. The GP_{CL} crystal structure suggests that the glycan cap may act as a final layer of defense, shielding the critical and conserved NPC1 domain C binding site from host immune surveillance prior to cellular entry. We show that this RBS has a crest-and-trough morphology and exists at the apex of the GP_{CL} trimer.

The crest is lined with hydrophilic basic residues, while the trough is recessed and entirely hydrophobic. Mutagenic analysis of EBOV GP_{CL} demonstrates that the crest is involved in nonspecific electrostatic interactions with NPC1, requiring an overall basic charge to facilitate binding of NPC1 domain C. Mutations in EBOV GP (such as K114E+K115E) that reverse the electrostatic charge on the GP_{CL} crest consistently abrogate receptor binding and reduce infectivity. In contrast, the GP_{CL} trough is involved in more specific hydrophobic interactions with NPC1 domain C. Structure-based mutants with mutations designed to obstruct the structure of the trough (such as T83M+I113M) diminish the affinity of GP for NPC1 domain C and severely restrict the infectivity of VSV pseudotypes bearing these mutations. Based on the crystal structure and results of mutagenesis reported here, we propose that the NPC1 receptor binds GP in a two-stage process. First, GP_{CL} recruits the NPC1 domain C receptor through nonspecific electrostatic interactions between NPC1 and the basic crest region on GP_{CL}. Without this interaction, there is no detectable GP-receptor binding. Next, specific hydrophobic interactions are initiated between the GP_1 RBS trough and NPC1 domain C. The specificity of these interactions likely explains the differential effects of individual mutations in the trough (Fig. 3 and 4), whereas the effects of mutations in the crest were determined by charge, not specific amino acid position.

We also further analyzed two mutants with a mutation in the hydrophobic trough, F88A or L111A, which have been described previously as unable to support infection (25, 26). These two mutants are outliers in our analysis. Their infectivities are reduced by more than three $\log_{10}$ infectious units relative to that of WT EBOV GP, despite only modest defects in binding of NPC1 domain C. We postulate that these mutants are defective at a step downstream from NPC1 binding. They will provide useful tools to further decipher precisely how GP_{CL}-NPC1 binding facilitates fusion triggering and membrane fusion.

Recent work has identified multiple neutralizing MAbs from a patient who survived MARV infection. The MAbs from those studies were found to bind to the apex of MARV GP_1 (11, 22)—the site we have confirmed here to be the filovirus GP_1 receptor-binding site. Since ebolavirus, marburgvirus, and cuevavirus GP proteins all use the NPC1 protein as a receptor, it is not unexpected that the structure of the GP_1 RBS would be highly conserved across all filoviruses (10, 17–19, 32). Thus, we hypothesized that the MAbs identified by Flyak et al. (22), shown to target the RBS trough on MARV GP_1 (11), should be broadly neutralizing. However, unlike the GP proteins of marburgviruses, those of the ebolaviruses and cuevavirus maintain a glycan cap structure that effectively shields the GP_1 RBS from immune surveillance. Therefore, by proteolytically priming filovirus GPs on the surface of VSV particles (such as VSV-EBOV GP_{CL}), we were able to analyze the neutralization potential of MAbs targeting the otherwise-occluded filovirus RBS. Analysis of GP_{CL}-bearing VSVs would tell us if it was worthwhile to target such antibodies to the endosome as future therapeutics.

Of the panel of neutralizing MAbs from an MARV survivor described by Flyak et al. (22), only one, MR72, demonstrates significant cross-reactivity to uncleaved EBOV GP. Three other MAbs, MR78, MR111, and MR191, only react with EBOV GP_{CL}. We focused our analysis on the EBOV GP-reactive MR72 and the EBOV GP_{CL}-reactive MR78 and MR191, which approach GP from different angles. Here, we show that MR72 effectively neutralizes VSV pseudovirions bearing GP_{CL} from EBOV, SUDV, BDBV, TAFV, RESTV, or LLOV. MR191 neutralizes the EBOV, BDBV, TAFV, and LLOV VSV-GP_{CL} virions weakly (and RESTV and SUDV GP_{CL} not at all), with infectivity never reduced below 50% (see Fig. S3 in the supplemental material). In contrast, MR78 can only neutralize MARV GP_{CL}. It cannot neutralize EBOV GP_{CL}-bearing VSVs, even though it is able to bind them.

The crystal structures of MARV GP_{CL} and EBOV GP_{CL} bound to MR78 suggest that MR78 binds the same site in both viruses. However, the resolution of the EBOV GP_{CL}-MR78 complex was too low to identify subtle differences imposed by sequence deviations from MARV GP that might explain why MR78 fails to neutralize EBOV GP_{CL} (11). Hence, we used a panel of VSV-EBOV GP RBS mutants to understand which sequence variations could prevent MR78-mediated neutralization of EBOV GP_{CL}. Surprisingly, the introduction of a single point mutation (V79A) within the EBOV RBS allows MR78 to neutralize VSV-EBOV GP_{CL}-V79A. Of significance, BDBV, TAFV, and RESTV GPs also encode valine at this position, while SUDV and LLOV GPs encode isoleucine and leucine, respectively. The larger Val, Ile, and Leu aliphatic residues encoded by the ebolaviruses and cuevavirus may prevent MR78 from neutralizing their GP_{CL}-bearing particles (Fig. 4A; see also Fig. S3 in the supplemental material). We note that, unlike MR78, MR191 exhibits no improvement in neutralization of VSV-EBOV GP_{CL}-V79A (see Fig. S3 in the supplemental material). How MR72 but not MR78 is able to overcome divergent amino acids at position 79 to broadly neutralize filovirus GP_{CL} is the subject of continued structural and biochemical study.

Remarkably, enhanced neutralization of EBOV GP_{CL}-V79A by MR78 was not accompanied by a commensurate increase in its capacity to block NPC1 binding of this GP (Fig. 4). This apparent uncoupling of neutralization and receptor blockage raises the possibility that MR78 may act as an allosteric inhibitor, preventing membrane fusion by binding to GP_1 subunits in the trimer that are not occupied by NPC1 domain C in the endosome. There, it may inhibit events that occur after receptor binding in order to trigger GP-mediated membrane fusion. Mutations like L111A, which eliminate infectivity without affecting receptor binding, may target these same post-receptor-binding steps.

Recent events, including the unprecedented EBOV epidemic in West Africa (3, 34), coinciding with human cases of MARV emerging in central Africa (35) and the emergence of BDBV (36) and re-emergence of SUDV (37) in this decade, highlight the urgent need for broad-spectrum antifilovirus therapeutics (38). Here, we demonstrate that the highly conserved binding site for the essential intracellular receptor NPC1 provides an attractive and underexplored target for broadly protective antibodies or small-molecule therapeutics. However, one crucial challenge to the development of such antibodies as therapeutics is an evolved feature of the filovirus entry mechanism—the unavailability of its NPC1-binding site to extracellular antibodies. The success of this

antiviral strategy therefore requires novel protein engineering approaches to deliver GP_{CL}-specific MAbs to late endosomes and/or lysosomes, where the NPC1-binding site is unmasked by host proteases.

MATERIALS AND METHODS

Expression and purification of GP_{CL}-KZ52 complex for crystallization. Ebola virus GP (lacking the mucin domain [residues 312 to 462]) was produced by stable expression in *Drosophila melanogaster* S2 cells. Briefly, Effectene (Qiagen) was used to transfect S2 cells with a modified pMT-puro vector plasmid containing the GP gene of interest, followed by stable selection of transfected cells with 6 μg/ml puromycin. Cells were cultured at 27°C in complete Schneider's medium for selection and then adapted to Insect Xpress medium (Lonza) for large-scale expression in 2-liter Erlenmeyer flasks. Secreted GP ectodomain expression was induced with 0.5 mM $CuSO_4$, and supernatant harvested after 4 days. Ebola virus GP was engineered with a double Strep-tag at the C terminus to facilitate purification using Strep-Tactin resin (2-1201-010) (Qiagen) and then further purified by Superdex 200 size exclusion chromatography (SEC) in 10 mM Tris-buffered saline (Tris-HCl, pH 7.5, 150 mM NaCl [TBS]). EBOV GP_{CL} was produced by incubation of 1 mg GP with 0.02 mg thermolysin overnight at room temperature in TBS containing 1 mM $CaCl_2$ and purified by using Superdex 200 SEC. Trimeric EBOV GP_{CL} was then complexed with a KZ52 Fab fragment prior to crystallization as previously described (4).

Crystallization, data collection, and structure determinations. The purified EBOV GP_{CL}-KZ52 Fab complex was concentrated to 3.5 mg/ml in TBS. The crystal drops consisted of a 1:1 ratio of protein/well solution. The well solution consisted of 25% polyethylene glycol monomethyl ether 550 (PEG MME 550), 10% 2-propanol, 5% ethylene glycol, 100 mM sodium acetate, pH 4.7, and 100 mM calcium chloride. Crystals grew over the course of a month and were flash frozen directly out of the crystal drop into liquid nitrogen for data collection. Data were collected remotely at the Argonne National Laboratory, Advanced Photon Source (APS), from the GM/CA beamline 23-ID-D. The structure was determined using molecular replacement with PHASER (39), within the CCP4 suite (40), using a modified EBOV GP-KZ52 complex model (PDB code 3CSY) with all the residues corresponding to the glycan cap removed (4). Refinement of the EBOV GP_{CL} crystal structure was done through iterative cycles of model building using COOT, followed by refinement with Refmac5 and PHENIX (41–43). Translation/libration/screw (TLS) motion was applied during refinement with the TLS Motion Determination (TLSMD) server used to determine the TLS structure partitions (44, 45). Five percent of the data was set aside prior to refinement for the R_{free} calculations for each data set (46). The statistics and stereochemistry of the crystal structure were checked using the MolProbity server until ranking at least at the >95th percentile (see Fig. S2A in the supplemental material) (47). All of the structural figures were rendered using PyMOL (PyMOL Molecular Graphics System, version 1.5.0.4; Schrödinger, LLC).

Cells and viruses. African grivet monkey kidney (Vero) cells were maintained at 37°C and 5% CO_2 in high-glucose Dulbecco's modified Eagle medium (DMEM; Invitrogen Corp., Carlsbad, CA) supplemented with 10% fetal calf serum. Replication-incompetent vesicular stomatitis virus (VSV) (serotype Indiana) pseudotyped viruses were generated as previously described (49). The wild type (VSV-WT GP) encodes enhanced green fluorescence protein (eGFP) in place of the VSV-G gene to allow scoring of infection and bears the EBOV GPΔmuc gene (Mayinga isolate, GenBank accession number AF086833) but lacks the mucin-like domain (residues 309 to 489 [Δmuc]) (6). Point mutants and multiple mutants were generated by subcloning GP fragments containing the mutation(s) to replace EBOV GPΔmuc. Cleaved VSV-GP_{CL} particles were generated by incubating VSV-GP pseudotypes with thermolysin (250 μg/ml) for 1 h at 37°C. The reaction was stopped by adding phosphoramidon (1 mM) and incubating on ice for 5 min.

Normalization of GP for ELISA. Normalization of GP_{CL} amounts to be used in the binding experiments was done by ELISA, as illustrated in Fig. S4 in the supplemental material. Briefly, high-binding 96-well ELISA plates (Corning) were coated with serial dilutions of GP_{CL} in phosphate-buffered saline (PBS), and allowed to bind at 37°C for 1 h. The plates were blocked with PBS containing 3% bovine serum albumin (PBSA), followed by incubation with the anti-GP monoclonal antibody KZ52 (2 μg/ml in PBS) (21) and a horseradish-conjugated anti-human secondary antibody (Santa Cruz Biotechnology), which was detected by ultra-TMB (3,3′,5,5′-tetramethylbenzidine) substrate (Thermo Scientific). Absorbance readings were subjected to a nonlinear regression analysis (GraphPad Prism software) to generate binding curves and calculate an EC_{50} value. Additionally, the virions were normalized for GP incorporation by comparing the amount of GP to the amount of the VSV matrix protein (M). Equal amounts of purified virions were resolved on SDS-PAGE and blotted for the VSV matrix protein using a mouse anti-VSV M antibody (23H12). Quantification was done using a LI-COR IR dye-conjugated anti-mouse Alexa Fluor 680 secondary antibody (Invitrogen) on the Odyssey Imaging Station and Image Studio 2.1 software (LI-COR Biosciences), and the results were normalized to the WT control. Virus particles that had less than 25% incorporation of mutant GP compared to the incorporation of WT GP or that were highly sensitive to proteolysis were excluded from our analysis.

GP-NPC1 domain C capture ELISA. Binding of GP to NPC1 domain C was performed as previously described (10, 32). Briefly, high-binding 96-well ELISA plates (Corning) were coated with the anti-GP monoclonal antibody KZ52 (2 μg/ml in PBS) (21). Following a blocking step, either uncleaved or *in vitro*-cleaved GP_{CL} pseudotypes were captured on the plate. Unbound GP was washed off, and serial dilutions of Flag-tagged purified soluble human NPC1 domain C (0 to 40 μg/ml) were added. Bound NPC1 domain C was detected by a horseradish-conjugated anti-Flag antibody (Sigma-Aldrich), using ultra-TMB substrate (Thermo Scientific). EC_{50}s were calculated from binding curves generated by nonlinear regression analysis using GraphPad Prism software. Binding ELISAs were done in duplicate in at least two independent experiments. All incubation steps were done at 37°C for 1 h or at 4°C overnight.

Pseudovirus neutralization assays. Serial dilutions of MAbs and of a no-antibody control were mixed with either cleaved or uncleaved VSV-GP particles and allowed to bind for 1 h at room temperature. Monolayers of Vero cells were inoculated with the antibody-virus mixture in duplicate and incubated at 37°C in 5% CO_2. Infection was scored 12 to 16 h postinfection by enumeration of eGFP-positive cells under a fluorescence microscope. The ZMapp cocktail MAbs 2G4, 4G7, and 13C6, as well as MAb KZ52, prepared as previously described (33), were generously provided by Mapp Biopharmaceutical. MAbs MR78 and MR72 were prepared as previously described (22).

Protein structure accession number. Coordinates and structure factors have been deposited into the Protein Data Bank under accession number 5HJ3.

SUPPLEMENTAL MATERIAL

Supplemental material for this article may be found at http://mbio.asm.org/lookup/suppl/doi:10.1128/mBio.02154-15/-/DCSupplemental.

Figure S1, PDF file, 2.7 MB.
Figure S2, PDF file, 0.3 MB.
Figure S3, PDF file, 1.2 MB.
Figure S4, PDF file, 0.2 MB.

ACKNOWLEDGMENTS

We thank the beamline scientists at GM/CA 23-ID for support during data collection.

E.O.S. was supported by NIAID R01 AI101436 and R01 AI081982 and an Investigators in the Pathogenesis of Infectious Disease award from the Burroughs Wellcome Fund. K.C. acknowledges support from NIAID R01 AI088027 and R01 AI101436, and J.E.C. was supported by NIAID U19

AI109711 and by the Defense Threat Reduction Agency (HDTRA1-13-1-0034).

FUNDING INFORMATION

HHS | NIH | National Institute of Allergy and Infectious Diseases (NIAID) provided funding to Erica Ollmann Saphire under grant numbers R01 AI101436 and R01 AI081982. HHS | NIH | National Institute of Allergy and Infectious Diseases (NIAID) provided funding to Kartik Chandran under grant numbers R01 AI088027 and R01 AI101436. HHS | NIH | National Institute of Allergy and Infectious Diseases (NIAID) provided funding to James E. Crowe under grant number U19 AI109711. DOD | Defense Threat Reduction Agency (DTRA) provided funding to James E. Crowe under grant number HDTRA1-13-1-0034.

REFERENCES

1. **De la Vega MA, Stein D, Kobinger GP.** 2015. Ebolavirus evolution: past and present. PLoS Pathog **11:**e1005221. http://dx.doi.org/10.1371/journal.ppat.1005221.
2. **Negredo A, Palacios G, Vázquez-Morón S, González F, Dopazo H, Molero F, Juste J, Quetglas J, Savji N, de la Cruz Martínez M, Herrera JE, Pizarro M, Hutchison SK, Echevarría JE, Lipkin WI, Tenorio A.** 2011. Discovery of an ebolavirus-like filovirus in Europe. PLoS Pathog **7:**e1002304. http://dx.doi.org/10.1371/journal.ppat.1002304.
3. **Baize S, Pannetier D, Oestereich L, Rieger T, Koivogui L, Magassouba N, Soropogui B, Sow MS, Keïta S, De Clerck H, Tiffany A, Dominguez G, Loua M, Traoré A, Kolié M, Malano ER, Heleze E, Bocquin A, Mély S, Raoul H, Caro V, Cadar D, Gabriel M, Pahlmann M, Tappe D, Schmidt-Chanasit J, Impouma B, Diallo AK, Formenty P, Van Herp M, Gunther S.** 2014. Emergence of Zaire Ebola virus disease in Guinea. N Engl J Med **371:**1418–1425. http://dx.doi.org/10.1056/NEJMoa1404505.
4. **Lee JE, Fusco ML, Hessell AJ, Oswald WB, Burton DR, Saphire EO.** 2008. Structure of the Ebola virus glycoprotein bound to an antibody from a human survivor. Nature **454:**177–182. http://dx.doi.org/10.1038/nature07082.
5. **Lee JE, Saphire EO.** 2009. Neutralizing ebolavirus: structural insights into the envelope glycoprotein and antibodies targeted against it. Curr Opin Struct Biol **19:**408–417. http://dx.doi.org/10.1016/j.sbi.2009.05.004.
6. **Jeffers SA, Sanders DA, Sanchez A.** 2002. Covalent modifications of the Ebola virus glycoprotein. J Virol **76:**12463–12472. http://dx.doi.org/10.1128/JVI.76.24.12463-12472.2002.
7. **Kaletsky RL, Simmons G, Bates P.** 2007. Proteolysis of the Ebola virus glycoproteins enhances virus binding and infectivity. J Virol **81:**13378–13384. http://dx.doi.org/10.1128/JVI.01170-07.
8. **Schornberg K, Matsuyama S, Kabsch K, Delos S, Bouton A, White J.** 2006. Role of endosomal cathepsins in entry mediated by the Ebola virus glycoprotein. J Virol **80:**4174–4178. http://dx.doi.org/10.1128/JVI.80.8.4174-4178.2006.
9. **Chandran K, Sullivan NJ, Felbor U, Whelan SP, Cunningham JM.** 2005. Endosomal proteolysis of the Ebola virus glycoprotein is necessary for infection. Science **308:**1643–1645. http://dx.doi.org/10.1126/science.1110656.
10. **Miller EH, Obernosterer G, Raaben M, Herbert AS, Deffieu MS, Krishnan A, Ndungo E, Sandesara RG, Carette JE, Kuehne AI, Ruthel G, Pfeffer SR, Dye JM, Whelan SP, Brummelkamp TR, Chandran K.** 2012. Ebola virus entry requires the host-programmed recognition of an intracellular receptor. EMBO J **31:**1947–1960. http://dx.doi.org/10.1038/emboj.2012.53.
11. **Hashiguchi T, Fusco ML, Bornholdt ZA, Lee JE, Flyak AI, Matsuoka R, Kohda D, Yanagi Y, Hammel M, Crowe JE, Jr., Saphire EO.** 2015. Structural basis for Marburg virus neutralization by a cross-reactive human antibody. Cell **160:**904–912. http://dx.doi.org/10.1016/j.cell.2015.01.041.
12. **Mulherkar N, Raaben M, de la Torre JC, Whelan SP, Chandran K.** 2011. The Ebola virus glycoprotein mediates entry via a non-classical dynamin-dependent macropinocytic pathway. Virology **419:**72–83. http://dx.doi.org/10.1016/j.virol.2011.08.009.
13. **Saeed MF, Kolokoltsov AA, Albrecht T, Davey RA.** 2010. Cellular entry of Ebola virus involves uptake by a macropinocytosis-like mechanism and subsequent trafficking through early and late endosomes. PLoS Pathog **6:**e1001110. http://dx.doi.org/10.1371/journal.ppat.1001110.
14. **Mingo RM, Simmons JA, Shoemaker CJ, Nelson EA, Schornberg KL, D'Souza RS, Casanova JE, White JM.** 2015. Ebola virus and severe acute respiratory syndrome coronavirus display late cell entry kinetics: evidence that transport to NPC1+ endolysosomes is a rate-defining step. J Virol **89:**2931–2943. http://dx.doi.org/10.1128/JVI.03398-14.
15. **Nanbo A, Imai M, Watanabe S, Noda T, Takahashi K, Neumann G, Halfmann P, Kawaoka Y.** 2010. Ebolavirus is internalized into host cells via macropinocytosis in a viral glycoprotein-dependent manner. PLoS Pathog **6:**e1001121. http://dx.doi.org/10.1371/journal.ppat.1001121.
16. **Dube D, Brecher MB, Delos SE, Rose SC, Park EW, Schornberg KL, Kuhn JH, White JM.** 2009. The primed ebolavirus glycoprotein (19-kilodalton GP1,2): sequence and residues critical for host cell binding. J Virol **83:**2883–2891. http://dx.doi.org/10.1128/JVI.01956-08.
17. **Carette JE, Raaben M, Wong AC, Herbert AS, Obernosterer G, Mulherkar N, Kuehne AI, Kranzusch PJ, Griffin AM, Ruthel G, Dal Cin P, Dye JM, Whelan SP, Chandran K, Brummelkamp TR.** 2011. Ebola virus entry requires the cholesterol transporter Niemann-Pick C1. Nature **477:**340–343. http://dx.doi.org/10.1038/nature10348.
18. **Côté M, Misasi J, Ren T, Bruchez A, Lee K, Filone CM, Hensley L, Li Q, Ory D, Chandran K, Cunningham J.** 2011. Small molecule inhibitors reveal Niemann-Pick C1 is essential for Ebola virus infection. Nature **477:**344–348. http://dx.doi.org/10.1038/nature10380.
19. **Krishnan A, Miller EH, Herbert AS, Ng M, Ndungo E, Whelan SP, Dye JM, Chandran K.** 2012. Niemann-Pick C1 (NPC1)/NPC1-like1 chimeras define sequences critical for NPC1's function as a flovirus entry receptor. Viruses **4:**2471–2484. http://dx.doi.org/10.3390/v4112471.
20. **Herbert AS, Davidson C, Kuehne AI, Bakken R, Braigen SZ, Gunn KE, Whelan SP, Brummelkamp TR, Twenhafel NA, Chandran K, Walkley SU, Dye JM.** 2015. Niemann-Pick C1 is essential for ebolavirus replication and pathogenesis in vivo. mBio **6:**e00565-15. http://dx.doi.org/10.1128/mBio.00565-15.
21. **Maruyama T, Rodriguez LL, Jahrling PB, Sanchez A, Khan AS, Nichol ST, Peters CJ, Parren PW, Burton DR.** 1999. Ebola virus can be effectively neutralized by antibody produced in natural human infection. J Virol **73:**6024–6030.
22. **Flyak AI, Ilinykh PA, Murin CD, Garron T, Shen X, Fusco ML, Hashiguchi T, Bornholdt ZA, Slaughter JC, Sapparapu G, Klages C, Ksiazek TG, Ward AB, Saphire EO, Bukreyev A, Crowe JE, Jr.** 2015. Mechanism of human antibody-mediated neutralization of Marburg virus. Cell **160:**893–903. http://dx.doi.org/10.1016/j.cell.2015.01.031.
23. **Bale S, Liu T, Li S, Wang Y, Abelson D, Fusco M, Woods VL, Jr., Saphire EO.** 2011. Ebola virus glycoprotein needs an additional trigger, beyond proteolytic priming for membrane fusion. PLoS Negl Trop. Dis **5:**e1395. http://dx.doi.org/10.1371/journal.pntd.0001395.
24. **Brindley MA, Hughes L, Ruiz A, McCray PB, Jr., Sanchez A, Sanders DA, Maury W.** 2007. Ebola virus glycoprotein 1: identification of residues important for binding and postbinding events. J Virol **81:**7702–7709. http://dx.doi.org/10.1128/JVI.02433-06.
25. **Manicassamy B, Wang J, Jiang H, Rong L.** 2005. Comprehensive analysis of Ebola virus GP1 in viral entry. J Virol **79:**4793–4805. http://dx.doi.org/10.1128/JVI.79.8.4793-4805.2005.
26. **Mpanju OM, Towner JS, Dover JE, Nichol ST, Wilson CA.** 2006. Identification of two amino acid residues on Ebola virus glycoprotein 1 critical for cell entry. Virus Res **121:**205–214. http://dx.doi.org/10.1016/j.virusres.2006.06.002.
27. **Martinez O, Ndungo E, Tantral L, Miller EH, Leung LW, Chandran K, Basler CF.** 2013. A mutation in the Ebola virus envelope glycoprotein restricts viral entry in a host species- and cell-type-specific manner. J Virol **87:**3324–3334. http://dx.doi.org/10.1128/JVI.01598-12.
28. **Miller EH, Harrison JS, Radoshitzky SR, Higgins CD, Chi X, Dong L, Kuhn JH, Bavari S, Lai JR, Chandran K.** 2011. Inhibition of Ebola virus entry by a C-peptide targeted to endosomes. J Biol Chem **286:**15854–15861. http://dx.doi.org/10.1074/jbc.M110.207084.
29. **Miller EH, Chandran K.** 2012. Filovirus entry into cells—new insights. Curr Opin Virol **2:**206–214. http://dx.doi.org/10.1016/j.coviro.2012.02.015.
30. **Dias JM, Kuehne AI, Abelson DM, Bale S, Wong AC, Halfmann P, Muhammad MA, Fusco ML, Zak SE, Kang E, Kawaoka Y, Chandran K, Dye JM, Saphire EO.** 2011. A shared structural solution for neutralizing ebolaviruses. Nat Struct Mol Biol **18:**1424–1427. http://dx.doi.org/10.1038/nsmb.2150.
31. **Murin CD, Fusco ML, Bornholdt ZA, Qiu X, Olinger GG, Zeitlin L, Kobinger GP, Ward AB, Saphire EO.** 2014. Structures of protective

antibodies reveal sites of vulnerability on Ebola virus. Proc Natl Acad Sci U S A **111:**17182–17187. http://dx.doi.org/10.1073/pnas.1414164111.

32. **Ng M, Ndungo E, Jangra RK, Cai Y, Postnikova E, Radoshitzky SR, Dye JM, Ramírez de Arellano E, Negredo A, Palacios G, Kuhn JH, Chandran K.** 2014. Cell entry by a novel European filovirus requires host endosomal cysteine proteases and Niemann-Pick C1. Virology **468–470:**637–646. http://dx.doi.org/10.1016/j.virol.2014.08.019.
33. **Qiu X, Wong G, Audet J, Bello A, Fernando L, Alimonti JB, Fausther-Bovendo H, Wei H, Aviles J, Hiatt E, Johnson A, Morton J, Swope K, Bohorov O, Bohorova N, Goodman C, Kim D, Pauly MH, Velasco J, Pettitt J, Olinger GG, Whaley K, Xu B, Strong JE, Zeitlin L, Kobinger GP.** 2014. Reversion of advanced Ebola virus disease in nonhuman primates with ZMapp. Nature **514:**47–53. http://dx.doi.org/10.1038/nature13777.
34. **Carroll MW, Matthews DA, Hiscox JA, Elmore MJ, Pollakis G, Rambaut A, Hewson R, García-Dorival I, Bore JA, Koundouno R, Abdellati S, Afrough B, Aiyepada J, Akhilomen P, Asogun D, Atkinson B, Badusche M, Bah A, Bate S, Baumann J, Becker D, Becker-Ziaja B, Bocquin A, Borremans B, Bosworth A, Boettcher JP, Cannas A, Carletti F, Castilletti C, Clark S, Colavita F, Diederich S, Donatus A, Duraffour S, Ehichioya D, Ellerbrok H, Fernandez-Garcia MD, Fizet A, Fleischmann E, Gryseels S, Hermelink A, Hinzmann J, Hopf-Guevara U, Ighodalo Y, Jameson L, Kelterbaum A, Kis Z, Kloth S, Kohl C, Korva M.** 2015. Temporal and spatial analysis of the 2014–2015 Ebola virus outbreak in West Africa. Nature **524:**97–101. http://dx.doi.org/10.1038/nature14594.
35. **Maganga GD, Kapetshi J, Berthet N, Kebela Ilunga B, Kabange F, Mbala Kingebeni P, Mondonge V, Muyembe JJ, Bertherat E, Briand S, Cabore J, Epelboin A, Formenty P, Kobinger G, González-Angulo L, Labouba I, Manuguerra JC, Okwo-Bele JM, Dye C, Leroy EM.** 2014. Ebola virus disease in the Democratic Republic of the Congo. N Engl J Med **371:**2083–2091. http://dx.doi.org/10.1056/NEJMoa1411099.
36. **Towner JS, Sealy TK, Khristova ML, Albariño CG, Conlan S, Reeder SA, Quan PL, Lipkin WI, Downing R, Tappero JW, Okware S, Lutwama J, Bakamutumaho B, Kayiwa J, Comer JA, Rollin PE, Ksiazek TG, Nichol ST.** 2008. Newly discovered Ebola virus associated with hemorrhagic fever outbreak in Uganda. PLoS Pathog **4:**e1000212. http://dx.doi.org/10.1371/journal.ppat.1000212.
37. **Shoemaker T, MacNeil A, Balinandi S, Campbell S, Wamala JF, McMullan LK, Downing R, Lutwama J, Mbidde E, Ströher U, Rollin PE, Nichol ST.** 2012. Reemerging Sudan Ebola virus disease in Uganda, 2011. Emerg Infect Dis **18:**1480–1483. http://dx.doi.org/10.3201/eid1809.111536.
38. **Mylne A, Brady OJ, Huang Z, Pigott DM, Golding N, Kraemer MU, Hay SI.** 2014. A comprehensive database of the geographic spread of past human Ebola outbreaks. Sci Data **1:**140042. http://dx.doi.org/10.1038/sdata.2014.42.
39. **McCoy AJ, Grosse-Kunstleve RW, Adams PD, Winn MD, Storoni LC, Read RJ.** 2007. Phaser crystallographic software. J Appl Crystallogr **40:**658–674. http://dx.doi.org/10.1107/S0021889807021206.
40. **Collaborative Computational Project Number 4.** 1994. The CCP4 suite: programs for protein crystallography. Acta Crystallogr D Biol Crystallogr **50:**760–763. http://dx.doi.org/10.1107/S0907444994003112.
41. **Emsley P, Cowtan K.** 2004. Coot: model-building tools for molecular graphics. Acta Crystallogr D Biol Crystallogr **60:**2126–2132. http://dx.doi.org/10.1107/S0907444904019158.
42. **Evans P.** 2006. Scaling and assessment of data quality. Acta Crystallogr D Biol Crystallogr **62:**72–82. http://dx.doi.org/10.1107/S0907444905036693.
43. **Adams PD, Afonine PV, Bunkóczi G, Chen VB, Davis IW, Echols N, Headd JJ, Hung LW, Kapral GJ, Grosse-Kunstleve RW, McCoy AJ, Moriarty NW, Oeffner R, Read RJ, Richardson DC, Richardson JS, Terwilliger TC, Zwart PH.** 2010. PHENIX: a comprehensive python-based system for macromolecular structure solution. Acta Crystallogr D Biol Crystallogr **66:**213–221. http://dx.doi.org/10.1107/S0907444909052925.
44. **Painter J, Merritt EA.** 2006. Optimal description of a protein structure in terms of multiple groups undergoing TLS motion. Acta Crystallogr D Biol Crystallogr **62:**439–450. http://dx.doi.org/10.1107/S0907444906005270.
45. **Painter J, Merritt EA.** 2006. TLSMD web server for the generation of multi-group TLS models. J Appl Crystallogr **39:**109–111. http://dx.doi.org/10.1107/S0021889805038987.
46. **Brünger AT.** 1992. Free R-value—a novel statistical quantity for assessing the accuracy of crystal-structures. Nature **355:**472–475. http://dx.doi.org/10.1038/355472a0.
47. **Chen VB, Arendall WB, Headd JJ, Keedy DA, Immormino RM, Kapral GJ, Murray LW, Richardson JS, Richardson DC.** 2010. MolProbity: all-atom structure validation for macromolecular crystallography. Acta Crystallogr D Biol Crystallogr **66:**12–21. http://dx.doi.org/10.1107/S0907444909042073.
48. **Baker NA, Sept D, Joseph S, Holst MJ, McCammon JA.** 2001. Electrostatics of nanosystems: application to microtubules and the ribosome. Proc Natl Acad Sci U S A **98:**10037–10041. http://dx.doi.org/10.1073/pnas.181342398.
49. **Takada A, Robison C, Goto H, Sanchez A, Murti KG, Whitt MA, Kawaoka Y.** 1997. A system for functional analysis of Ebola virus glycoprotein. Proc Natl Acad Sci U S A **94(26):**14764–14769.